Automatic Target Recognition Via Passive Radar, Using Precomputed Radar Cross Sections and a Coordinated Flight Model

Lisa M. Ehrman and Aaron D. Lanterman

The authors are with the School of Electrical and Computer Engineering, Georgia Institute of Technology, Mail Code 0250, Atlanta, GA 30332 (e-mail: {lanterma,ehrman}@ece.gatech.edu).

This work was funded by the NATO Consultation, Command, and Control Agency (NC3A), as well as by start-up funds from the School of Electrical and Computer Engineering at the Georgia Institute of Technology. The authors would like to thank Dr. Paul Howland and Dr. Rene van der Heiden at NC3A for their support. They would also like to thank Major Larkin Hastriter and Lt. Col. Adam MacDonald for their assistance in obtaining aircraft flight paths. Finally, the authors would like to thank Professor Lakshmi Sankar of the School of Aerospace Engineering at the Georgia Institute of Technology for his patience and guidance.

Abstract

Rather than emitting pulses, passive radar systems rely on illuminators of opportunity to illuminate potential targets. These systems are particularly attractive since they allow receivers to operate without emitting energy, rendering them covert. Many existing passive radar systems estimate the locations of targets. This paper focuses on adding an automatic target recognition (ATR) component to such systems.

The proposed approach to ATR compares the Radar Cross Section (RCS) of targets detected by a passive radar system to the precomputed RCS of known targets. To effectively use this approach, the precomputed RCS must be accurately modeled. This is accomplished through the use of the Fast Illinois Solver Code (FISC), a coordinated flight model, the Numerical Electromagnetic Code (NEC2) and the Advanced Refractive Effects Prediction System (AREPS). The resulting precomputed RCS corresponds to a particular aircraft in the target class executing the desired maneuver while being illuminated by the passive radar system. A Rician likelihood model compares the RCS of the detected target to the precomputed RCS of known targets in the target class. Target identification results from this comparison.

Results are presented for a variety of possible aircraft flight paths, and system configurations. Algorithm performance appears to be affected by the aircraft trajectory, the accuracy of the aircraft position estimates, and the achieved signal-to-noise ratio (SNR). The results are generally quite good at the anticipated noise levels when the aircraft position is accurately known; however, significant performance degradation is noted for one aircraft type when the HH polarized antennas are used.

I. INTRODUCTION

A. History of the Problem

There are two parallel schools of thought prevalent in the literature regarding the recognition of fast-moving fixed-wing aircraft. The first approach proposes the creation of target images, such as two-dimensional inverse synthetic aperture radar (ISAR) images or a sequence of one-dimensional range profiles [1]. Target recognition is then conducted using these images. The alternate approach has been to bypass the creation of images and attempt recognition directly from the received data. Following the path suggested in [2], Herman takes this second approach to automatic target recognition (ATR), using data obtained from a passive radar system [3], [4].

Although ATR has been a subject of much research, Herman's application of passive radar was innovative. Unlike traditional radar systems, passive radar systems bypass the need for dedicated transmitters by exploiting "illuminators of opportunity" such as commercial television and FM radio signals. In doing so, they are able to reap a number

of benefits. Most notably, the fact that passive radar systems do not emit energy renders them covert; this is a great strategic advantage if the systems are employed by the military. Passive radar systems also alleviate potential problems relating to spectral availability. Someone wishing to build a passive radar system must only take advantage of transmitters in the area, rather than obtaining permits for an ever more densely populated radar spectrum.

It is also noteworthy that many illuminators of opportunity employ low frequencies. Although passive radar systems do not inherently require these low frequencies, the allocation of bandwidth for commercial TV and FM radio implies that passive radar systems operate at lower frequencies than traditional microwave radar. As a fortunate though unintended consequence, the low-frequency signals exploited by passive radar are well-suited for ATR [5], [6], [7]. In addition to being less susceptible to inclement weather, the longer wavelengths result in target radar cross sections that vary "slowly" with small changes in the target state vector. Herman noted that the variation in radar cross section (RCS), as characterized by the number of nulls encountered as a target's aspect changes, is proportional to the electrical length of the target [3], [4]. At FM-band frequencies (100 MHz), a fighter-sized aircraft is approximately five wavelengths long. In contrast, at the X-band frequencies used by many traditional radars (10 GHz), the same aircraft would be 500 wavelengths long, making the ATR system very sensitive to small changes in target orientation.

Despite its numerous benefits, passive radar was once deemed impractical. In the mid-1980s, Griffiths and Long [8] attempted to extract range information from backscattered television signals. Plagued by the low signal-to-noise ratio resulting from the available equipment and the range ambiguity inherent in the sync pulses of an analog TV signal, their results did not seem encouraging. A decade later, Howland [9] successfully tracked targets by abandoning any attempt to directly measure range in favor of the velocity information contained in the Doppler-shifted TV carrier and the angle-of-arrival information derived from a simple two-antenna array. Exotic track initialization algorithms, combined with an extended Kalman filter, fuse the Doppler and angle-of-arrival information into Cartesian coordinate tracks.

Today, several passive radar systems are in operation. The most widely tested manifestation of this kind of technology is probably the Silent Sentry series developed by Lockheed Martin Mission Systems of Gaithersburg, MD, which can exploit both analog television and FM radio signals. Another well-known system is the Manastash Ridge Radar[1] developed by John Sahr at the University of Washington [10], [11], which uses FM radio-based passive radar for atmospheric studies.

B. An Alternative Approach to ATR

The primary goal of this research is to add ATR capabilities to existing passive radar systems, using RCS as the key information for classification. Since RCS is highly aspect-dependent, accurate estimation of target orientation is crucial. Herman [3], [4] met this challenge with a computationally intensive particle filter [12], which jointly estimated target position, orientation, and target type. The major contribution of this paper is that it demonstrates that good results are often possible using a much simpler approach. In place of a particle filter, this approach uses a coordinated flight model [13] to estimate aircraft orientation from the aircraft flight path.

A database of Fast Illinois Solver Code (FISC) results is created for each aircraft in the target class. This database is accessed using the incident and observed azimuths and elevations, which can be computed once the aircraft orientation is known. The combination of the FISC database and coordinated flight model allows for the generation of a set of precomputed radar cross sections, corresponding to each aircraft in the target class executing the desired maneuver. These profiles are then scaled for propagation losses and antenna gain of the receiver using the Advanced Refractive Effects Prediction System (AREPS) and Numerical Electromagnetic Code (NEC2), respectively. Finally, the profiles corresponding to members of the target class are compared to the profile of the actual target, resulting in target identification.

The work presented here is simulation-based. Target profiles arriving at the receiver are simulated by adding white Gaussian noise to the profile. One hundred such noisy profiles are created for each member of the target class for each scenario to create a statistically significant set of simulations. It is worth noting that the aircraft comprising

[1] www-rcs.ee.washington.edu/~radar/Projects/Manastash

the target classes are chosen based upon the availability of acceptable CAD models, rather than likelihood of occurrence near a real system. A secondary goal of this research is to model a system currently being developed by NATO/NC3A with the intent of an eventual comparison with real data. At that point, more realistic target classes will be implemented.

II. Modeling RCS

A. System Description

The system parameters used in this work are selected to model a passive radar demonstration currently being developed by NATO. Table I shows the relevant parameters for the transmitter and receiver modeled in this research. To provide further insight into the viability of the algorithm, the simulations provided in this paper are conducted for both vertically polarized and horizontally polarized scenarios.

TABLE I

Transmitter and receiver parameters.

Parameter	Transmitter	Receiver
Latitude (N)	52^o 01' 00"	52^o 06' 36"
Longitude (E)	05^o 03' 00"	04^o 19' 26"
Altitude (m ASL)	375	100
Frequency (MHz)	100	–
Peak Power (kW)	100	–
Direction	Omni-Directional	320^o
Polarization	Vertical	Vertical

B. Estimating Aircraft Orientation with a Coordinated Flight Model

Given that target RCS is the sole factor used to classify the aircraft, its accurate representation is paramount. This is not a trivial task, as RCS is heavily dependent upon the incident and observed angles, which in turn are dependent upon the yaw, heading, pitch, and roll of the aircraft. Our response to this challenge implements a coordinated flight model to estimate these angles, given a set of time-correlated aircraft positions.

This process is described at length in other sources [13], [14]; thus, only the results will be presented here.

Since this research is primarily concerned with fast-moving fixed-wing aircraft, yaw is always assumed to be zero. This does not imply that aircraft direction goes unmeasured; it simply means that the aircraft nose is assumed to be oriented in the direction of motion. Aircraft heading, a far more revealing parameter, is expressed as,

$$\xi = \begin{cases} 90 - \arctan(\frac{v_Y}{v_X}), x > 0 \\ 270 - \arctan(\frac{v_Y}{v_X}), x < 0 \end{cases}, \tag{1}$$

where v_X and v_Y are the x and y components of aircraft velocity. The equation of pitch also follows from the assumption that the aircraft nose is pointed in the direction of motion, and is expressed as,

$$\theta = \arctan\left(\frac{dz}{\sqrt{dx^2 + dy^2}}\right), \tag{2}$$

where (dx, dy, dz) is the difference in aircraft position in the x, y, and z directions over an incremental period of time, dt. Finally, the aircraft roll is estimated as,

$$\phi = \arctan\left(\frac{|v|^2 \cos(\theta)}{Rg}\right), \tag{3}$$

where $|v|$ is the magnitude of the aircraft velocity, R is the instantaneous radius of curvature of the aircraft turn, and g is the standard gravity at Earth's surface.

The estimated aircraft orientation angles are appended to the aircraft positions, creating a supplemented flight profile. This is then used to determine the incident and observed angles, upon which RCS depends.

C. Modeling Target Radar Cross Section

Modeling the precomputed RCS of known targets in the target class is a multi-step process. The supplemented flight profile, containing aircraft position and orientation, is used to determine the incident and observed angles at every point during the encounter. The incident and observed angles are then used to access a database of FISC results which are available for each aircraft model in the target class. A set of power profiles are created when data is extracted from the RCS database. Additional scaling is required to make

these power profiles represent the signals arriving at the receiver due to the illuminated targets. Some significant factors that must be considered are propagation losses between the aircraft and antennas, and antenna gain. The propagation losses, which include effects due to multipath and terrain, are modeled using AREPS. As is likely to be the case for most passive radar applications, the transmitting antenna exploited by the NATO system is omni-directional. Thus, the only antenna gain pattern that must be modeled corresponds to the receiver; this modeling is accomplished with NEC2. To cut down on the length of time required to execute the simulation, databases are also created for AREPS and NEC2. The overall result of this process is a power profile that is scaled to account for propagation losses and antenna gain.

The necessity of the FISC database, as well as its limitations, are worth mentioning. Ideally, the simulation process described here would run FISC for every new set of incident and observed angles. However, the lengthy run-time and massive memory requirements of FISC render this option unfeasible. A more attractive option is the creation of a database of FISC results, in which aircraft RCS is sampled sufficiently to meet the Nyquist sampling criterion. In particular, the angular sampling of the RCS should satisfy,

$$\Delta\theta \leq \frac{c}{(2f_0)(size)}, \tag{4}$$

where c is the speed of light, f_0 is the radar frequency, and $size$ is the longest dimension of the aircraft [15]. The minimum angular sampling required for each aircraft when the frequency is 100 MHz is shown in Table II.

TABLE II

MINIMUM ANGULAR SAMPLING REQUIRED FOR EACH AIRCRAFT IN TARGET CLASS.

Aircraft	Longest Dim. (m)	Min. Spacing (^{o})
F-15	19.3	4.5
Falcon-20	17.1	5.0
Falcon-100	13.7	6.2
T-38	14.0	6.2

Using an angular spacing of 4^o, a database of FISC runs can be created that is sufficiently

full to represent the RCS of each aircraft type in the study, without aliasing. This database can be quickly accessed and allows for the creation of a power profile for virtually any desired flight path.

Although the profiles simulated by FISC are sampled as sparsely as possible while avoiding aliasing, the amount of time required to create a sufficiently large database remains daunting. At this point, the database has been completed for all combinations of observed azimuths and elevations, and incident azimuths. However, the incident elevations available in the database[2] are currently limited to $\pm 20^o$. Sparse sampling techniques will eventually be implemented to circumvent this limitation.

D. Modeling the Power Arriving at the Receiver

Recall that one goal of this research is to model a system currently being developed by NATO. Eventually, real power profiles may be available from the NATO receiver. Until then, it is necessary to simulate these profiles.

Two small changes differentiate this process from that used to find the precomputed RCS of known targets in the target class. First, when simulating the RCS of detected targets, the simulation is run with the real aircraft orientations in place of the estimated ones. These power profiles are then corrupted with additive white Gaussian noise, which acts independently on the real and imaginary parts of the signal. Along these lines, the simulated received profile is expressed as,

$$P_{SIM} = (\sqrt{P_R} + w_R)^2 + w_I^2, \tag{5}$$

where P_R is the real component of the power profile prior to being corrupted by noise, and w is zero-mean additive white Gaussian noise, which has real and imaginary components, w_R and w_I [4]. The noise power is computed in dBW using,

$$P_N = \frac{kT_0N_F}{CPI}, \tag{6}$$

[2]FISC requires a great deal of computational time to find the currents on the aircraft for a particular set of incident angles; however, once the model has been created for the set of incident angles, all of the possible pairs of observed angles can be computed relatively quickly. For this reason, the limited parameter in our database is the incident elevation.

where k is Boltzmann's constant, T_0 is temperature in Kelvin, N_F is the unitless noise figure, and CPI is the coherent processing interval of the system [16]. To match the NATO system, the CPI is set equal to 0.5 seconds, and T_0 is set equal to 290 K.

Selection of the noise figure, N_F, is more difficult. If the noise figure is only expected to account for thermal noise and out-of-band interference, then a conservative estimate of the noise figure in a city environment might be 30 dB. In the absence of data regarding the noise power of the NATO system, it is reasonable to use this approximation.

E. Noise Power Due to Direct Path Interference

The noise figure accounts for thermal noise and out-of-band interference, but until now the issue of transmitter interference has not been addressed. Typically, this direct path interference manifests itself as a spike in the cross-ambiguity function. Since the transmitter's power and location are known, and since the direct path interference spike occurs along the axis with zero velocity, this spike can usually be identified and removed. The more treacherous effect of transmitter interference is that is can raise the "thumbtack" noise floor of the ambiguity function, potentially masking the target spike. To be thorough, this should also be considered when computing the noise figure.

If the ambiguity function is normalized such that the direct path spike has unit height, then the average pedestal height, or sideband power, is given by

$$P_{pedestal} = \frac{1}{B \times CPI}, \tag{7}$$

where B is the signal bandwidth, and CPI is the coherent processing interval [17]. To match the NATO system, values of 45 kHz and 0.5 seconds are used for B and CPI, respectively. If propagation losses and antenna gain are neglected, the pedestal power is 44 dBW below the direct-path spike. Since the NATO transmitter power is 50 dBW, the sideband power is 6 dBW. Propagation losses and antenna gain play a significant role, lowering the pedestal power by 95 dBW. The electronics in the receiver of the NATO system also mitigate the problem by suppressing the direct path signal by 70 dBW, which reduces the sideband power to -159 dBW. More sophisticated filters could be implemented to further reduce the noise figure, but using the specifications of the system being modeled, the effective noise figure falls between 40 and 45 dB. Thus, the effects due to transmitter

interference are far more significant than those due to thermal noise and out-of-band interference.

To gain further insight into the impact of noise on the algorithm, the noise figure is swept from 30 dB to 100 dB in increments of 5 dB. Note that noise figures above 45 dB are not anticipated in a real setting; they are merely included in this paper to demonstrate the breaking point of the classification algorithm.

F. Target Classification

The simulation process is repeated for each member of the target class, resulting in a set of simulated radar cross sections corresponding to the detected targets. The automatic target recognizer compares these noisy received profiles to the library of precomputed power profiles. Equation 5 leads to a Rician likelihood model [4] whose probability density function is given by

$$p_x(x) = \frac{x}{\sigma_w^2} e^{\left(\frac{x^2+s^2}{2\sigma_w^2}\right)} I_0\left[\frac{xs}{\sigma_w^2}\right]. \tag{8}$$

To apply the Rician to the simulated and truth profiles, associate x with the magnitude of the RCS of the detected target, and s with the magnitude of the precomputed RCS of the target in the target class. The noise power, which equals the noise variance, is then equated with σ_w^2. If each point in time is considered an independent sample from a process, then the data loglikelihood is

$$\ln(p_x(\bar{x})) = \sum_{i=1}^{n} \ln\left(I_0\left[\frac{x_i s_i}{\sigma_w^2}\right]\right) - \left(\frac{x_i^2 + s_i^2}{2\sigma_w^2}\right). \tag{9}$$

Loglikelihoods are computed for each member of the target class; the target is identified as the member of the target class with the largest loglikelihood [18].

III. Results Obtained Using VV Antennas

Three scenarios of increasing complexity are presented to the algorithm. These maneuvers are drawn to scale relative to the antenna locations in Figure 1.

The first scenario consists of a simple straight-and-level flight path. This does little to test the coordinated flight model, but gives a good indication that the remainder of the algorithm is working. To be thorough, two straight-and-level trajectories have been

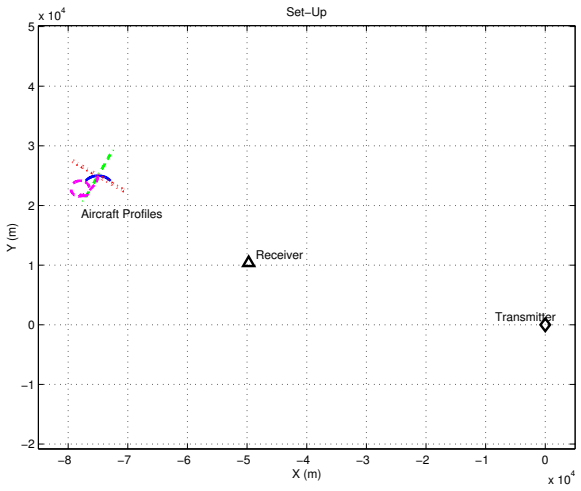

Fig. 1. Maneuver locations relative to system transmitter and receiver.

tested. The aircraft in the first trajectory flies away from the receiver, while the aircraft in the second trajectory flies broadside to the receiver. Notable differences in the results are observed.

The next scenario implements a constant-altitude, circular banked turn. Although this circular banked turn is not a realistic flight trajectory, it indicates that the algorithm is able to perform when the aircraft power profiles become more complex. It also provides a more strenuous test of the coordinated flight model than the straight-and-level trajectories.

Finally, a flight profile recorded on-board a maneuvering F-15 at Edwards Air Force Base[3] is used to provide a more realistic test of the algorithm. The Edwards trajectory came complete with measured aircraft orientation, allowing a unique opportunity to quantify the performance degradation induced from having to estimate aircraft orientation. First, the algorithm is executed with the real aircraft orientation angles used in place of the ones estimated by the coordinated flight model. This serves as a baseline for comparison. Next, the simulation is run using the estimated aircraft orientation angles. Finally, a test is conducted in which the aircraft position is errantly estimated to be 300 m north and 300 m west of its actual location. This gauges performance degradation due to errors in the position estimates.

[3]The F-15C trajectory was obtained from the Joint Helmet Cuing System, Mission JH-16, conducted by the 445th Flight Test Squadron at Edwards Air Force Base in May 2000.

A. Straight-and-Level Trajectory # 1

The straight-and-level trajectory used in the first scenario contains targets moving at 200 m/s with altitudes of 8000 m. Recall that the targets in this maneuver are moving directly away from the receiver. As a relatively small number of aspects of the aircraft are visible to the receiver, it stands to reason that this represents a challenging scenario for the classification algorithm. The library profiles resulting from this maneuver are shown in Figure 2a. The four profiles are expected to look less similar when more aspects are presented to the receiver. The sharp dip in the profiles around 42 seconds is also worthy of comment. This might be troublesome if it were generated by FISC, but it is actually attributed to AREPS and the process used to model propagation.

The noise figure is swept from 30 dB to 100 dB, in increments of 5 dB, to gauge performance degradation as a function of noise power. One-hundred runs are executed using each aircraft as the detected target, for each noise figure. The percentage of incorrect identifications (probability of error) obtained for each aircraft model at each noise level is shown in Figure 2b. This data is obtained from a set of Monte Carlo runs; thus the jumps in the curves are artificial and are expected to smooth out as the number of samples increase.

Comparison of the probability of error plot with the plot of the power profiles provides insight into the viability of the algorithm. Figure 2a demonstrates that the algorithm performs perfectly until the noise figure reaches 50 dB. This corresponds to noise power of -151 dBW. Using the plot of the power profiles in Figure 2a, it is clear that this noise power is approximately equal to the maximum power of the signal. Once again, better performance might be expected if the power profiles looked less similar. This is likely to be the case when the aircraft flies broadside to the receiver, as more aspects will be presented to the receiver.

It is also noteworthy that the probability of error at high noise figures, for all four aircraft, is in the ballpark of 75%. This implies that when the signal is buried in the noise, the odds of the algorithm correctly identifying an aircraft are one in four; since there are four aircraft models in the target class, this is equivalent to chance.

Confusion matrices are tabulated to provide further insight into the types of mistakes

being made by the algorithm. The aircraft listed in the first column correspond to the aircraft detected by the receiver. The aircraft listed across the top row pertain to the aircraft identified by the algorithm. The confusion matrices for this encounter, with noise figures of 50, 55, and 60 dB are shown in Tables III through V.

B. Straight-and-Level Trajectory # 2

The straight-and-level trajectory is then translated to a new location and rotated such that the aircraft flies broadside to the receiver. This seemingly minor change has a significant effect on the shape of the power profiles and, in turn, on algorithm performance. The power profiles and probability of error plots are shown in Figures 3a and 3b, respectively.

With this change in trajectory, the algorithm is able to correctly identify the aircraft at much higher noise levels. For example, the algorithm began misidentifying the F-15 in the first straight-and-level maneuver when the noise figure was 50 dB; here, in contrast, the algorithm does not begin incorrectly identifying the F-15 until the noise figure reaches 80 dB. The better performance is attributed to two factors. The primary cause is that the shape of the F-15 power profile is much more distinct from the other power profiles. A secondary factor is that the amplitude of the power profiles is larger, meaning that more noise is required to swamp the signal. These factors contribute to a lesser degree to the better performance with the Falcon-100. In the case of the other two aircraft, however, the power profiles look very similar to each other. This, coupled with the lack of increased signal amplitude, explains the lack of improved performance identifying the Falcon-20 and T-38A.

The confusion matrices for this maneuver, shown in Tables VI through VIII, reveal a dramatic pattern. Consider the first confusion matrix, for which the noise figure is 55 dB. Figure 3b demonstrates that the only aircraft misidentified by the algorithm at this noise level are the T-38A and Falcon-20. The confusion matrix reveals that the misidentification errors are limited to swapping the T-38A and Falcon-20. Neither of these aircraft are mistakenly identified as the F-15 or Falcon-100. This pattern continues in Table VII. In this case, the only aircraft not being misidentified is the F-15. As before, the T-38A, Falcon-20, and Falcon-100, though misidentified by the algorithm, are never misidentified as the F-15. This pattern implies that the algorithm's main error is to swap aircraft

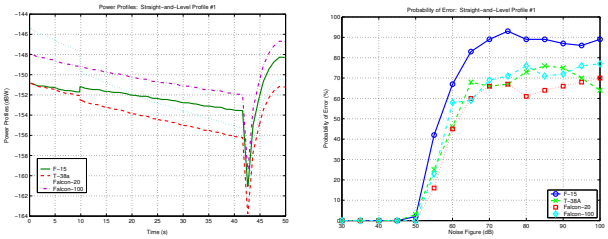

Fig. 2. Straight-and-level flight profile #1: a.) power profiles (left), b.) probability of error vs. noise nigure (right).

TABLE III

CONFUSION MATRIX FOR STRAIGHT-AND-LEVEL TRAJECTORY #1 WITH NOISE FIGURE = 50 DB.

Aircraft	F-15	T-38A	Falcon-20	Falcon-100
F-15	98	1	0	1
T-38A	3	97	0	0
Falcon-20	0	0	100	0
Falcon-100	0	0	0	100

TABLE IV

CONFUSION MATRIX FOR STRAIGHT-AND-LEVEL TRAJECTORY #1 WITH NOISE FIGURE = 55 DB.

Aircraft	F-15	T-38A	Falcon-20	Falcon-100
F-15	58	24	3	15
T-38A	21	75	3	1
Falcon-20	1	5	84	10
Falcon-100	14	3	6	77

TABLE V

CONFUSION MATRIX FOR STRAIGHT-AND-LEVEL TRAJECTORY #1 WITH NOISE FIGURE = 60 DB.

Aircraft	F-15	T-38A	Falcon-20	Falcon-100
F-15	33	34	13	20
T-38A	20	54	13	13
Falcon-20	10	19	55	16
Falcon-100	22	13	23	42

whose power profiles have comparable amplitude. This swapping begins to occur when the maximum signal power generated by the aircraft becomes buried in the noise.

C. Bank-Turn Trajectory

The constant-altitude circular banked turn provides a more difficult test of the algorithm. In this case, the target velocity is 100 m/s, and the altitude is 8000 m. Like the straight-and-level profiles, this is an idealized maneuver, rather than one recorded during an actual flight. Unlike the straight-and-level maneuver, this trajectory requires the coordinated flight model to estimate non-zero aircraft roll. The power profiles and probability of error curves are shown in Figures 4a and 4b.

In this case, the maximum signal power is roughly -150 dBW for all four aircraft models. Thus, algorithm performance is expected to be excellent for all four aircraft until the noise figure rises above 50 dB. Figure 4b supports this claim. Also note that the probability of error curves are more tightly clustered around 75% at high noise levels than before. This is attributed to the fact that the power profiles generated by all four aircraft have comparable amplitudes. Using the pattern described in Section III-B, the swapping errors made by the algorithm are expected to encompass all four aircraft models. The confusion matrices, shown in Tables IX through XI, confirm this suspicion.

D. Edwards Trajectory

To gauge the performance of the algorithm when the target is maneuvering, the third test uses the Edwards trajectory. During the maneuver, the target changes altitudes and executes turns with varying degrees of curvature. This maneuver is shown in Figure 5 from both 3-D and 2-D perspectives, and was previously used to test the coordinated flight model.

To generate a baseline for comparison, this algorithm is first run using the known aircraft orientation angles. This essentially removes the coordinated flight model, and any error it induces, from the process. This test is then redone using the full algorithm, including the coordinated flight model. To simulate the possibility that the position estimates obtained from the passive radar system contain errors, a third test in conducted in which the estimated aircraft position is translated 300 m north and 300 m west. During this final

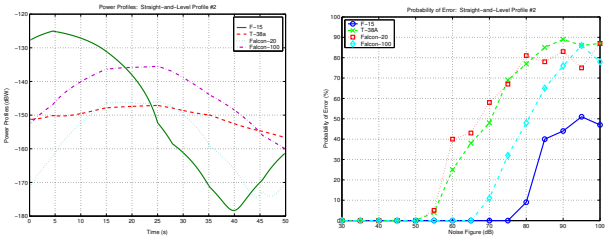

Fig. 3. Straight-and-level flight profile #2: a.) power profiles (left), b.) probability of error vs. noise figure (right).

TABLE VI

CONFUSION MATRIX FOR STRAIGHT-AND-LEVEL TRAJECTORY #2 WITH NOISE FIGURE = 55 DB.

Aircraft	F-15	T-38A	Falcon-20	Falcon-100
F-15	100	0	0	0
T-38A	0	96	4	0
Falcon-20	0	5	95	0
Falcon-100	0	0	0	100

TABLE VII

CONFUSION MATRIX FOR STRAIGHT-AND-LEVEL TRAJECTORY #2 WITH NOISE FIGURE = 70 DB.

Aircraft	F-15	T-38A	Falcon-20	Falcon-100
F-15	100	0	0	0
T-38A	0	52	40	8
Falcon-20	0	50	42	8
Falcon-100	0	2	9	89

TABLE VIII

CONFUSION MATRIX FOR STRAIGHT-AND-LEVEL TRAJECTORY #2 WITH NOISE FIGURE = 80 DB.

Aircraft	F-15	T-38A	Falcon-20	Falcon-100
F-15	91	3	0	6
T-38A	16	23	19	42
Falcon-20	15	24	19	42
Falcon-100	17	17	14	52

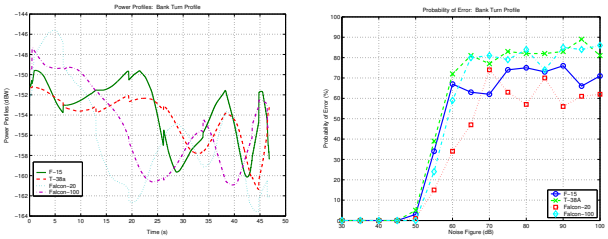

Fig. 4. Constant-altitude circular banked turn: a.) power profiles (left), b.) probability of error vs. noise figure (right).

TABLE IX

CONFUSION MATRIX FOR THE BANKED TURN TRAJECTORY WITH NOISE FIGURE = 50 DB.

Aircraft	F-15	T-38A	Falcon-20	Falcon-100
F-15	97	3	0	0
T-38A	5	95	0	0
Falcon-20	0	0	99	1
Falcon-100	0	0	0	100

TABLE X

CONFUSION MATRIX FOR THE BANKED TURN TRAJECTORY WITH NOISE FIGURE = 60 DB.

Aircraft	F-15	T-38A	Falcon-20	Falcon-100
F-15	33	19	22	26
T-38A	19	28	27	26
Falcon-20	4	9	66	21
Falcon-100	7	13	39	41

TABLE XI

CONFUSION MATRIX FOR THE BANKED TURN TRAJECTORY WITH NOISE FIGURE = 70 DB.

Aircraft	F-15	T-38A	Falcon-20	Falcon-100
F-15	38	22	23	17
T-38A	36	23	24	17
Falcon-20	32	22	26	20
Falcon-100	33	22	26	19

test, the algorithm attempts to recognize targets while assuming these incorrect position estimates are correct.

The power profiles and probability of error curves generated for the F-15 under the three different tests are shown in Figures 6a and 6b, respectively. Although the power profiles show some marked deviations when the orientation angles are estimated and when the position errors are included, the probability of error curves corresponding to the three tests are remarkably similar. In fact, there seems to be little degradation in performance due to using the coordinated flight model, even in the presence of position errors. This is also true for the T-38 and Falcon-100, whose plots are shown in Figures 7 and 8, respectively.

The only aircraft for which degradation in performance is noted is the Falcon-20. Even in this case, the performance is nearly identical when the estimated orientation angles are substituted for the actual ones. The only performance degradation occurs when the errant positions are used to estimate the orientation angles. The power profiles and probability of error plots for the Falcon-20 appear in Figure 9.

The confusion matrices obtained with a noise figure of 60 dB are shown in Tables XII through XIV. To get a better sense of the differences in algorithm performance between the three tests, we computed the percentage of total errors. For a noise figure of 60 dB, the algorithm is correct 97% of the time when the orientation angles are known, 92% of the time when the orientation angles are estimated from correct positions, and 90% of the time when incorrect position estimates are used.

Although performance degrades significantly when the noise figure increases to 70 dB, the results of the three tests remain similar to each other. At a noise figure of 70 dB, the algorithm is correct 46% of the time when the correct orientation angles are used, 49% of the time when the estimated orientation angles are used, and 46% of the time when incorrect positions are used to estimate the orientation angles. Confusion matrices corresponding to these three tests are displayed in Tables XV through XVII.

IV. Results Obtained Using HH Antennas

As in the previous section, three scenarios of increasing complexity are used to test the algorithm. The simplest of the three scenarios involves an aircraft flying in a straight-and-

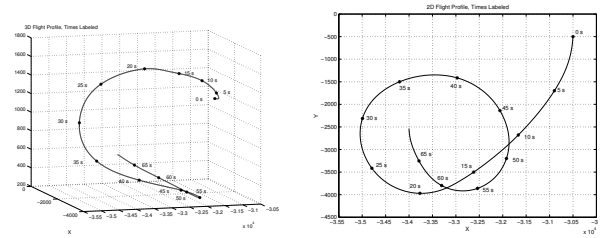

Fig. 5. F-15 maneuver: a) 3-D view (left), b) top view (right).

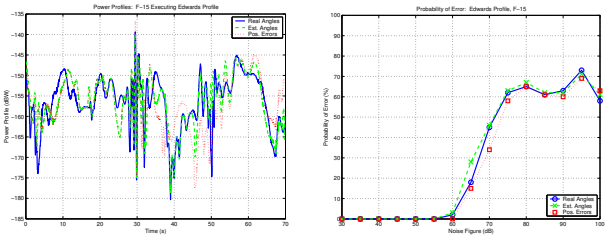

Fig. 6. F-15 executing the Edwards trajectory: a) power profiles (left), b) probability of error (right).

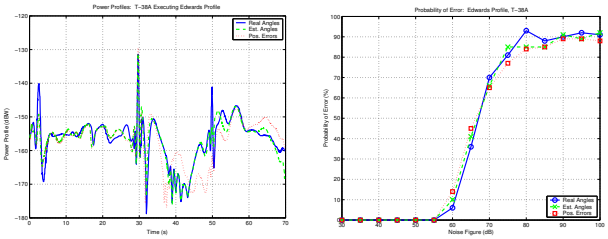

Fig. 7. T-38A executing the Edwards trajectory: a) power profiles (left), b) probability of error (right).

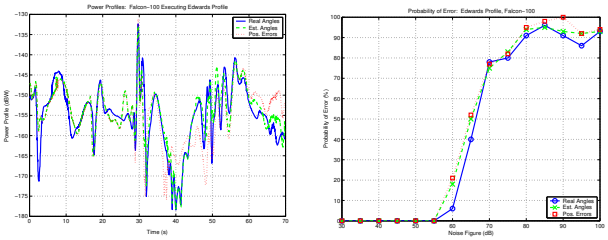

Fig. 8. Falcon-100 executing the Edwards trajectory: a) power profiles (left), b) probability of error (right).

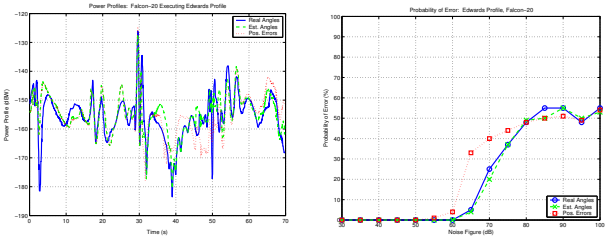

Fig. 9. Falcon-20 executing the Edwards trajectory: a) power profiles (left), b) probability of error (right).

TABLE XII

CONFUSION MATRIX FOR THE EDWARDS TRAJECTORY WITH NOISE FIGURE = 60 DB, USING REAL ORIENTATION ANGLES.

Aircraft	F-15	T-38A	Falcon-20	Falcon-100
F-15	98	0	0	2
T-38A	1	94	0	5
Falcon-20	0	0	100	0
Falcon-100	0	6	0	94

TABLE XIII

CONFUSION MATRIX FOR THE EDWARDS TRAJECTORY WITH NOISE FIGURE = 60 DB, USING ESTIMATED ORIENTATION ANGLES.

Aircraft	F-15	T-38A	Falcon-20	Falcon-100
F-15	97	1	0	2
T-38A	2	90	0	8
Falcon-20	0	0	100	0
Falcon-100	1	17	0	82

TABLE XIV

CONFUSION MATRIX FOR THE EDWARDS TRAJECTORY WITH NOISE FIGURE = 60 DB, USING INCORRECT POSITION ESTIMATES.

Aircraft	F-15	T-38A	Falcon-20	Falcon-100
F-15	100	0	0	0
T-38A	3	86	0	11
Falcon-20	0	1	96	3
Falcon-100	3	18	0	79

TABLE XV

CONFUSION MATRIX FOR THE EDWARDS TRAJECTORY WITH NOISE FIGURE = 70 DB, USING REAL ORIENTATION ANGLES.

Aircraft	F-15	T-38A	Falcon-20	Falcon-100
F-15	55	20	10	15
T-38A	31	30	21	18
Falcon-20	7	11	75	7
Falcon-100	32	25	21	22

TABLE XVI

CONFUSION MATRIX FOR THE EDWARDS TRAJECTORY WITH NOISE FIGURE = 70 DB, USING ESTIMATED ORIENTATION ANGLES.

Aircraft	F-15	T-38A	Falcon-20	Falcon-100
F-15	54	16	16	14
T-38A	27	34	22	17
Falcon-20	10	7	80	3
Falcon-100	30	24	21	25

TABLE XVII

CONFUSION MATRIX FOR THE EDWARDS TRAJECTORY WITH NOISE FIGURE = 70 DB, USING INCORRECT POSITION ESTIMATES.

Aircraft	F-15	T-38A	Falcon-20	Falcon-100
F-15	66	17	6	11
T-38A	36	35	13	16
Falcon-20	15	17	60	8
Falcon-100	37	27	13	23

level path directly away from the receiver. A variation of this maneuver is also conducted in which the aircraft heading is rotated by 90^o such that it flies broadside to the receiver. The aircraft in the second scenario executes a constant-altitude, constant-velocity, circular banked turn. Although this second maneuver is not terribly realistic, it provides a more strenuous test of the algorithm than the first maneuver, and builds the complexity of testing towards the final maneuver. The final maneuver used to test the algorithm is a flight profile recorded on-board a maneuvering F-15 at Edwards Air Force Base[4]. This Edwards trajectory was provided complete with measured aircraft orientation, allowing us a unique opportunity to quantify performance degradation attributed to the estimation of aircraft orientation. First, the measured orientation angles are used to establish a baseline for algorithm performance. Then, the simulation is redone using the estimated orientation angles in place of the real ones. Finally, to gauge performance degradation caused by errors in the position estimates, the test is redone using aircraft positions that are errantly estimated to be 300 m north and 300 m west of the actual locations. All of the maneuver trajectories are shown in Figure 1.

A. Straight-and-Level Trajectory # 1

The power profiles generated for all four aircraft in the target class are shown in Figure 10a. Since this simulation uses the same propagation loss profile as Section III-A, it contains the same dip at 42 seconds. The probability of error curve for this maneuver is shown in Figure 10b.

As is clear from Figure 10b, the algorithm performs perfectly when the noise figure is less than 50 dB. Errors in target identification are first noted for the F-15, T-38A, and Falcon-100 when the noise figure is 50 dB, and a rapid decline in performance is noted as the noise figure increases beyond 50 dB. Despite identification errors of the other three aircraft, the algorithm is able to perfectly identify the Falcon-20 for noise figures up to $N_F = 55$ dB. A quick glance at Figure 10a reveals the cause of the better performance. While the F-15, T-38A, and Falcon-100 have maximum signal power of approximately -155 dBW, the maximum signal power of the Falcon-20 is approximately -145 dBW. This

[4]The F-15C trajectory was obtained from the Joint Helmet Cuing System, Mission JH-16, conducted by the 445th Flight Test Squadron at Edwards Air Force Base in May 2000.

differentiates its profile from the others. As is the case when the antennas are vertically polarized, the more variations exist between the power profiles, the better the algorithm is able to identify the aircraft. Confusion matrices for this encounter, with noise figures of 50, 55, and 60 dB are shown in Tables XVIII through XX.

In addition to being the most likely aircraft to be correctly identified when present at these noise levels, the Falcon-20 is the least likely to be mistakenly identified as the target.

B. Straight-and-Level Trajectory # 2

The test is then repeated with the second straight-and-level trajectory. The effects of changing aircraft position and heading are largely dependent upon aircraft type. The maximum signal power of the F-15 rises from -155 dBW in the first encounter to approximately -145 dBW. The maximum signal power of the remaining three aircraft falls between -140 and -135 dBW.

Because this path shows a greater diversity of aspect angles on the target, we might expect performance in this encounter to improve for all of the aircraft models. A comparison of Figures 10b and 11b supports this claim. In this test, the algorithm performs perfectly for noise figures up to N_F= 60 dB. Once again, this is approximately the point at which the maximum noise power overtakes the maximum signal power.

The confusion matrices corresponding to noise figures of 65, 70, and 75 dB are shown in Tables XXI through XXIII. A familiar pattern emerges in these confusion matrices. For a noise figure of 55 dB, the algorithm does not just exhibit non-zero probability of error for the Falcon-20 and T-38A; when it misidentifies these two aircraft, it swaps them. This trend continues until the noise figure reaches 70 dB, the point at which the algorithm begins incorrectly identifying the Falcon-100. At that point, a small number of the T-38A and Falcon-20 cases begin to be misidentified as the Falcon-100. None of the aircraft are misidentified as the F-15 until the noise figure reaches 80 dB. Again, this corresponds to the point at which the algorithm begins to mistake the F-15 for other aircraft. In this case, the likelihood of an aircraft model being incorrectly classified as another model and the likelihood of being falsely identified occur at the same noise levels.

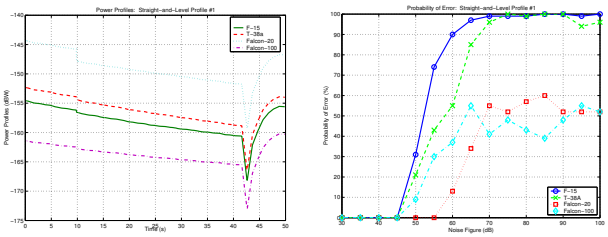

Fig. 10. Straight-and-level flight profile #1: a.) power profiles (left), b.) probability of error vs. noise figure (right).

TABLE XVIII

CONFUSION MATRIX FOR STRAIGHT-AND-LEVEL TRAJECTORY #1 WITH NOISE FIGURE = 50 DB.

Aircraft	F-15	T-38A	Falcon-20	Falcon-100
F-15	69	17	0	14
T-38A	21	79	0	0
Falcon-20	0	0	100	0
Falcon-100	9	0	0	91

TABLE XIX

CONFUSION MATRIX FOR STRAIGHT-AND-LEVEL TRAJECTORY #1 WITH NOISE FIGURE = 55 DB.

Aircraft	F-15	T-38A	Falcon-20	Falcon-100
F-15	26	36	0	38
T-38A	30	57	1	12
Falcon-20	0	0	100	0
Falcon-100	22	8	0	70

TABLE XX

CONFUSION MATRIX FOR STRAIGHT-AND-LEVEL TRAJECTORY #1 WITH NOISE FIGURE = 60 DB.

Aircraft	F-15	T-38A	Falcon-20	Falcon-100
F-15	10	36	5	49
T-38A	7	45	6	42
Falcon-20	0	13	87	0
Falcon-100	14	23	0	63

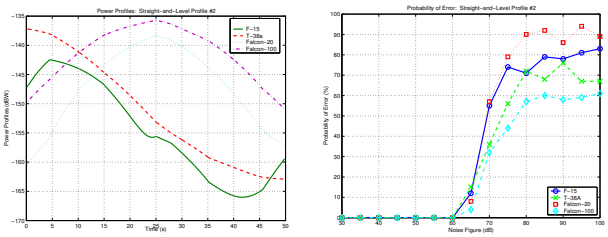

Fig. 11. Straight-and-level flight profile #2: a.) power profiles (left), b.) probability of error vs. noise figure (right).

TABLE XXI

CONFUSION MATRIX FOR STRAIGHT-AND-LEVEL TRAJECTORY #2 WITH NOISE FIGURE = 65 DB.

Aircraft	F-15	T-38A	Falcon-20	Falcon-100
F-15	88	9	3	0
T-38A	15	85	0	0
Falcon-20	4	1	92	3
Falcon-100	0	0	4	96

TABLE XXII

CONFUSION MATRIX FOR STRAIGHT-AND-LEVEL TRAJECTORY #2 WITH NOISE FIGURE = 70 DB.

Aircraft	F-15	T-38A	Falcon-20	Falcon-100
F-15	45	27	24	4
T-38A	16	64	14	6
Falcon-20	20	18	43	19
Falcon-100	2	7	23	68

TABLE XXIII

CONFUSION MATRIX FOR STRAIGHT-AND-LEVEL TRAJECTORY #2 WITH NOISE FIGURE = 75 DB.

Aircraft	F-15	T-38A	Falcon-20	Falcon-100
F-15	26	34	17	23
T-38A	19	44	14	23
Falcon-20	17	26	21	36
Falcon-100	8	21	15	56

C. Bank-Turn Trajectory

The library profiles resulting from the bank turn maneuver are shown in Figure 12a. The probability of error is shown as a function of noise figure in Figure 12b. This time, the maximum signal power from each of the four aircraft is approximately -145 dBW. This suggests that the performance will be similar for all four aircraft models. It seems unlikely that any of the aircraft will be favored over others. The confusion matrices, shown in Tables XXIV through XXVI, validate this prediction; the errors are more evenly distributed over the various aircraft models than in the second straight-and-level encounter.

D. Edwards Trajectory

Finally, the three tests conducted with the Edwards trajectory are redone with horizontally polarized transmit and receive antennas. Recall that the first test is a baseline in which the correct aircraft orientation angles are used to compute the library power profiles. The second test uses the coordinated flight model to estimate aircraft orientation, given the correct aircraft position profiles. The third test uses incorrect position estimates as well as the estimated orientations. The power profiles generated under all three tests for the F-15 are shown in Figure 13a. The corresponding probability of error curves are presented in Figure 13b. Performance is very similar under all three tests.

Similar plots are shown in Figures 14a and 14b, now using the T-38A as the true target. Once again, the algorithm performance is strikingly similar under all three conditions. This trend holds for the Falcon-100, whose curves are presented in Figure 15. The only time that any large difference in performance is noted amongst the three tests occurs when the Falcon-20 is used. In that case, the Falcon-20 is incorrectly identified as the Falcon-100 when the estimated orientation angles are used. The curves for the Falcon-20 are shown in Figure 16.

Confusion matrices for a noise figure of 60 dB are shown in Tables XXVII through XXIX. Averaged over all four aircraft types, the algorithm has an accuracy rate of 97% at this noise level when the aircraft orientation angles are known, 64% when the coordinated flight model is used to estimate aircraft orientation, and 70% when the incorrect position estimates are used. The gap in performance between the first and the second two cases is

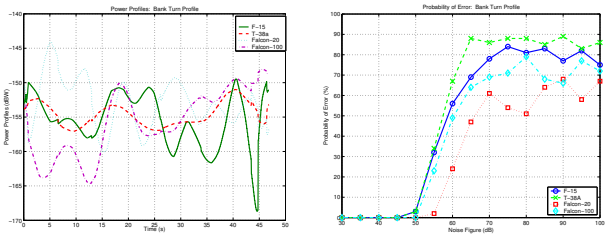

Fig. 12. Constant-altitude circular banked turn: a.) power profiles (left), b.) probability of error vs. noise figure (right).

TABLE XXIV

CONFUSION MATRIX FOR THE BANKED TURN TRAJECTORY WITH NOISE FIGURE = 50 DB.

Aircraft	F-15	T-38A	Falcon-20	Falcon-100
F-15	97	3	0	0
T-38A	3	97	0	0
Falcon-20	0	0	100	0
Falcon-100	0	0	0	100

TABLE XXV

CONFUSION MATRIX FOR THE BANKED TURN TRAJECTORY WITH NOISE FIGURE = 60 DB.

Aircraft	F-15	T-38A	Falcon-20	Falcon-100
F-15	44	19	14	23
T-38A	25	33	15	27
Falcon-20	8	10	76	6
Falcon-100	20	17	12	51

TABLE XXVI

CONFUSION MATRIX FOR THE BANKED TURN TRAJECTORY WITH NOISE FIGURE = 70 DB.

Aircraft	F-15	T-38A	Falcon-20	Falcon-100
F-15	22	14	36	28
T-38A	22	14	36	28
Falcon-20	22	11	39	28
Falcon-100	20	13	36	31

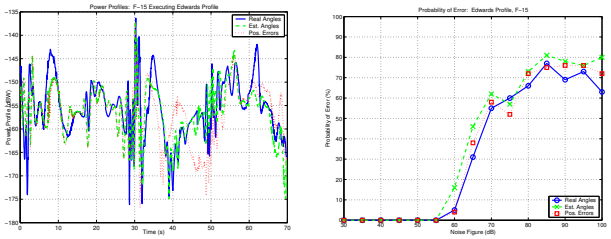

Fig. 13. F-15 executing the Edwards trajectory: a) power profiles (left), b) probability of error (right).

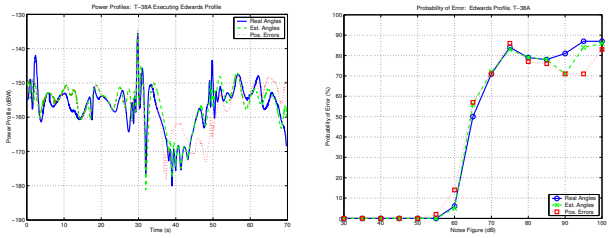

Fig. 14. T-38A executing the Edwards trajectory: a) power profiles (left), b) probability of error (right).

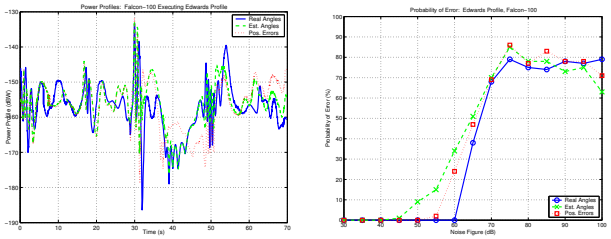

Fig. 15. Falcon-100 executing the Edwards trajectory: a) power profiles (left), b) probability of error (right).

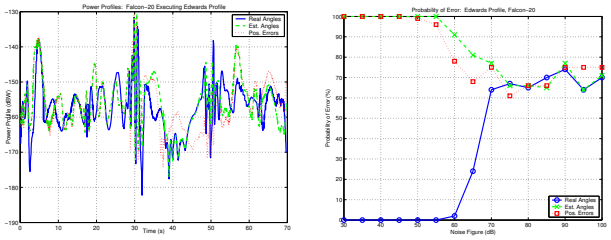

Fig. 16. Falcon-20 executing the Edwards trajectory: a) power profiles (left), b) probability of error (right).

largely due to the algorithm's difficulty with the Falcon-20. When the Falcon-20 is removed from the analysis, the accuracy rate of the algorithm is 96% using the correct orientation angles, 82% using the estimated orientation angles, and 86% using the incorrect position estimates. Note that using incorrect positions, in addition to incorrect orientations, seems to do better than using incorrect orientations with correct positions in these particular cases. This difference is probably not statistically significant.

As the noise figure increases to 70 dB, the results of all three tests become increasingly similar. Averaging over all four aircraft models, the algorithm has an accuracy rate of 36% when using the real orientation angles, 30% when using the estimated orientation angles, and 32% when the position estimates are incorrect. The confusion matrices corresponding to these three tests are shown in Tables XXX through XXXII.

Figure 16b vividly illustrates the difficulties which may arise from not estimating the orientation angles with enough accuracy; when using the estimated orientation angles at low noise levels, the Falcon-20 is *never* correctly identified. The Falcon-20 at the estimated orientation looks more like the Falcon-100 at the correct orientation than the Falcon-20 at the correct orientation! The model is so far off that increasing levels of noise actually yield better performance. In fact, the best performance, occurring at the *highest* noise levels, is that which would be achieved by randomly picking one of the four targets without looking at the data. To avoid such catastrophic model mismatches, we are currently exploring methods to jointly estimate the orientation and target type from the data.

V. Conclusion

Passive radar is an emerging technology that is only beginning to be exploited by the scientific community. The addition of ATR capabilities can only enhance the effectiveness of these systems. While this task was attempted by Herman with a particle filtering scheme, the major contribution of this paper is that it demonstrates that good results are often possible with a simpler approach.

The results presented in this paper provide a good deal of insight into the viability of this algorithm. Whether the maneuver is simple or complex, for the particular set of targets shown here, the ability to identify the aircraft model is largely dependent upon the maximum signal power being larger than the noise power. If 40 dB is truly a good estimate

TABLE XXVII

CONFUSION MATRIX FOR THE EDWARDS TRAJECTORY WITH NOISE FIGURE = 60 DB, USING REAL ORIENTATION ANGLES.

Aircraft	F-15	T-38A	Falcon-20	Falcon-100
F-15	95	3	1	1
T-38A	3	94	1	2
Falcon-20	0	1	98	1
Falcon-100	0	0	0	100

TABLE XXVIII

CONFUSION MATRIX FOR THE EDWARDS TRAJECTORY WITH NOISE FIGURE = 60 DB, USING ESTIMATED ORIENTATION ANGLES.

Aircraft	F-15	T-38A	Falcon-20	Falcon-100
F-15	84	15	0	1
T-38A	4	95	0	1
Falcon-20	0	15	9	76
Falcon-100	10	24	0	66

TABLE XXIX

CONFUSION MATRIX FOR THE EDWARDS TRAJECTORY WITH NOISE FIGURE = 60 DB, USING INCORRECT POSITION ESTIMATES.

Aircraft	F-15	T-38A	Falcon-20	Falcon-100
F-15	96	4	0	0
T-38A	11	86	0	3
Falcon-20	0	10	22	68
Falcon-100	12	12	0	76

TABLE XXX

CONFUSION MATRIX FOR THE EDWARDS TRAJECTORY WITH NOISE FIGURE = 70 DB, USING REAL ORIENTATION ANGLES.

Aircraft	F-15	T-38A	Falcon-20	Falcon-100
F-15	45	20	17	18
T-38A	36	29	21	14
Falcon-20	27	19	36	18
Falcon-100	30	20	18	32

TABLE XXXI

CONFUSION MATRIX FOR THE EDWARDS TRAJECTORY WITH NOISE FIGURE = 70 DB, USING ESTIMATED ORIENTATION ANGLES.

Aircraft	F-15	T-38A	Falcon-20	Falcon-100
F-15	38	18	21	23
T-38A	31	28	20	21
Falcon-20	23	15	23	39
Falcon-100	28	21	21	30

TABLE XXXII

CONFUSION MATRIX FOR THE EDWARDS TRAJECTORY WITH NOISE FIGURE = 70 DB, USING INCORRECT POSITION ESTIMATES.

Aircraft	F-15	T-38A	Falcon-20	Falcon-100
F-15	42	20	18	20
T-38A	30	29	21	20
Falcon-20	27	16	25	32
Falcon-100	30	16	23	31

of the noise figure, then the results obtained using this approach are encouraging. With the exception of the Falcon-20 case presented in Section IV-D, the identification results presented in this paper are perfect at the anticipated noise figure. Of course, we would not expect a real system to perform exactly as well as our simulations, since there will always be additional effects that cannot be easily modeled. However, the results do indicate that very good performance could be expected at the anticipated noise level.

The results obtained when both antennas are vertically polarized indicate that as long as the targets fall within the receiver's main lobe and are sufficiently close in range, the algorithm will have little trouble identifying them. Performance can then be expected to decline for aircraft whose trajectories do not cross through the receiver's main lobe, or whose position is too far away from the system to generate sufficient SNR. The range required to generate sufficient SNR is itself dependent upon the target type and orientation.

The results obtained using horizontally polarized antennas are slightly less encouraging, and indicate that the coordinated flight model should be tweaked as part of future work, to ensure excellent performance under a wide variety of conditions. An additional topic for future work is the expansion of the FISC database via sparse sampling techniques.

References

[1] S.P. Jacobs and J.A. O'Sullivan, "Automatic target recognition using sequences of high resolution radar range-profiles," *IEEE Trans. on Aerospace and Electronic Systems*, vol. 36, no. 2, pp. 364–382, 2000.

[2] A.D. Lanterman, "Tracking and recognition of airborne tagets via commercial television and fm radio signals," in *Acquisition, Tracking, and Pointing XIII*, M.K. Masten and L.A. Stockum, Eds., Orlando, FL, April 1999, vol. SPIE Proc. 3692, pp. 189–198.

[3] S.M. Herman, *A Particle Filtering Approach to Joint Passive Radar Tracking and Target Classification*, Doctoral Dissertation, Department of Electrical and Computer Engineering, Univ. of Illinois at Urbana-Champaign, Urbana, IL, 2002.

[4] S.C. Herman and P. Moulin, "A particle filtering approach to joint radar tracking and automatic target recognition," in *Proc. IEEE Aerospace Conference*, Big Sky, Montana, March 10-15 2002.

[5] Y.T. Lin and A.A. Ksienski, "Identification of complex geomtrical shapes by means of low-frequency radar returns," *The Radio and Electronic Engineer*, vol. 46, no. 10, pp. 472–486, Oct. 1976.

[6] H. Lin and A.A. Ksienski, "Optimum frequencies for aircraft classification," *IEEE Trans. on Aerospace and Electronic Systems*, vol. 17, no. 5, pp. 656–665, Sept. 1981.

[7] J.S. Chen and E.K. Walton, "Comparison of two target classification techniques," *IEEE Trans. on Aerospace and Electronic Systems*, vol. 22, no. 1, pp. 15–21, Jan. 1986.

[8] H.D. Griffiths and N.R.W. Long, "Television-based bistatic radar," *IEE Proceedings, Part F*, vol. 133, no. 7, pp. 649–657, December 1986.

[9] P.E. Howland, "Target tracking using television-based bistatic radar," *IEE Proc. F: Radar, Sonar, and Navigation*, vol. 146, no. 3, pp. 166–174, June 1999.

[10] J.D. Sahr and F.D. Lind, "The Manastash ridge radar: A passive bistatic radar for upper atmospheric radio science," *Radio Science*, pp. 2345–2358, Nov.-Dec. 1997.

[11] J.D. Sahr and F.D. Lind, "Passive radio remote sensing of the atmosphere using transmitters of opportunity," *Radio Science*, pp. 4–7, March 1998.

[12] A. Doucet, N. de Freitas, and N. Gordon, *Sequential Monte Carlo Methods in Practice*, Springer-Verlag, 2001.

[13] L. Ehrman and A.D. Lanterman, "Estimation of aircraft orientation from flight paths using a coordinated flight model," *submitted to IEEE Transactions on Aerospace and Electronic Systems*, November 2002.

[14] L.M. Ehrman, *Automatic Target Recognition Using Passive Radar and a Coordinated Flight Model*, Master's Thesis, School of Electrical and Computer Engineering, Georgia Institute of Technology, Atlanta, GA, 2003.

[15] D.L. Mensa, "Radar imaging," *International Journal of Imaging Systems and Technology*, vol. 4, pp. 148–163, 1992.

[16] D.K. Barton, *Modern Radar System Analysis*, Artech House, 1988.

[17] G. J. Frazer M. A. Ringer and S. J. Anderson, "Waveform analysis of transmitters of opportunity for passive radar," *Surveillance Systems Division, Electronics and Surveillance Research Laboratory.*

[18] L. Ehrman and A. Lanterman, "Automated target recogntion using passive radar and coordinated flight models," in *Automatic Target Recognition XIII*, Orlando, FL, April 2003, vol. SPIE Proc. 5094.